Horizontal–Longitudinal Spatial Correlation of Acoustic Field with Deep Receiver in the Direct Zone in Deep Water *

Kun-De Yang(杨坤德)[1,2]**, Hui Li(李辉)[1,2], Rui Duan(段睿)[1,2]

[1]School of Marine Science and Technology, Northwestern Polytechnical University, Xi'an 710072
[2]Key Laboratory of Ocean Acoustics and Sensing (Ministry of Industry and Information Technology), Northwestern Polytechnical University, Xi'an 710072

(Received 21 October 2016)

The horizontal–longitudinal correlation of acoustic field for the receiver near the bottom is analyzed by using numerical modeling. An approximate analytical solution of horizontal–longitudinal correlation coefficient is derived based on the ray method. Combining the characteristic of Lloyd's mirror interference pattern, the variability of acoustic field and its effect on horizontal–longitudinal spatial correlation are discussed. The theoretical prediction agrees well with the numerical results. Experimental results confirm the validity of analytical solution. Finally, the applicability of the analytical solution is summarized. The conclusion is beneficial for the design of bottom-moored array and the estimation of integral time for moving source localization.

PACS: 43.30.Cq, 43.30.Re DOI: 10.1088/0256-307X/34/2/024301

Both the spatial coherence length and temporal coherence time of sound transmission are important parameters for many practical sonar applications. The former is related to array gain and the latter is associated with temporal processing gain for the detection and localization of an acoustic signal. Practical requirements have promoted many experimental and theoretical studies of the signal coherence including both spatial and temporal coherence in deep water in the past few years. Gorodetskaya *et al.*[1] presented the results of combined consideration of sound coherence and array signal processing in long-range deep-water environments, and indicated that the large-array gain performance was inherently limited by the spatial coherence of multimode acoustic signal. Yang[2,3] reported the measurements of temporal coherence of acoustic signals propagating through shallow and deep water. Spiesberger[4] analyzed the temporal and spatial coherence of sound at 250 Hz and 1659 km in the Pacific Ocean. Colosi *et al.*[5] estimated the horizontal coherence functions using the transport theory based on a deep-water Philippine Sea environment. A horizontal coherence length of 1900 m in 500 km ranges with frequency of 75 Hz was obtained. Wu *et al.*[6] analyzed the experimental results for the horizontal correlation coefficients of acoustic signals obtained by a towed array in the West Pacific Ocean. Li *et al.*[7] analyzed the horizontal–longitudinal correlations in the convergence zones and the shadow zones based on the experimental data obtained in the South China Sea, and showed that the correlation length is consistent with the convergence zone width.

The reliable acoustic path (RAP) is an important acoustic duct with low transmission loss and high signal-to-noise ratio in the deep ocean. The physical properties of RAP environment have been analyzed and the source localization methods have been studied widely.[8–11] In this work, the horizontal–longitudinal correlation of acoustic field with deep receiver in the direct zone in deep water is investigated.

The horizontal–longitudinal correlation coefficient is used to describe the similarity of acoustic field in two ranges with the same receiver depth, which can be expressed in the frequency domain as[7]

$$\rho(r, r+\Delta r) = \max_{\tau} \frac{\mathrm{Re}[\int_{\omega_1}^{\omega_2} p_r(\omega) p^*_{r+\Delta r}(\omega) e^{i\omega\tau} d\omega]}{\sqrt{\int_{\omega_1}^{\omega_2} |p_r(\omega)|^2 d\omega \int_{\omega_1}^{\omega_2} |p_{r+\Delta r}(\omega)|^2 d\omega}}, \quad (1)$$

where $p_r(\omega)$ and $p_{r+\Delta r}(\omega)$ are the complex pressure fields in two separated ranges. The depth dependence is omitted from the notation of the pressure. Here Δr is the longitudinal separation between the two ranges, and ω_1 and ω_2 are the lower and upper angular frequencies of the acoustic field, respectively. The source spectrum is assumed to be 1 at all frequencies, τ is the compensatory time delay, $*$ represents the complex conjugation, and Re[·] is the real part.

In the simulation, a range-independent noise-free environment with water depth of 5000 m is assumed. A refracting Munk sound speed profile (SSP) is used. The sound channel axis depth and critical depth are 1200 m and 4430 m, respectively. The bottom is modeled by a half space with sound speed, density, and attenuation being 1500 m/s, 1.5 g/cm^3, and 0.14 dB/λ, respectively. Figure 1 shows transmission loss (TL) predicted with BELLHOP[12] at 310 Hz as a function of range and depth for a source at 100 m depth. The acoustic field of direct zone is dominated by the direct (D) and surface-reflected (SR) arrivals, resulting in the so-called Lloyd's mirror effect. The sea bottom also generates reflected arrivals, but we will not consider their effects due to the fact that the reflection losses of bottom-interacting arrivals are large.[10] Furthermore, the zone of interest in this

*Supported by the National Natural Science Foundation of China under Grant No 11174235.
**Corresponding author. Email: ykdzym@nwpu.edu.cn
© 2017 Chinese Physical Society and IOP Publishing Ltd

study is confined below the critical depth and within 30 km.

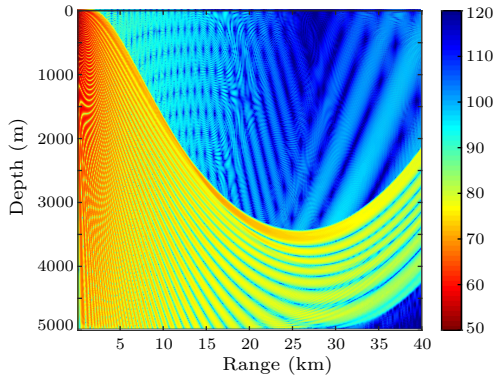

Fig. 1. TL predicted using BELLHOP for a source at 310 Hz and 100 m depth.

However, an actual deep ocean environment will likely have a variable sound speed profile; past works have shown that the image theory accurately describes the interference structure of the direct zone even in more complicated ocean environments. According to the image theory, the total field can be written simply as the sum of contributions of D and SR arrival. Based on the ray theory, the addition of the two contributions can be described as

$$p_r(\omega) = A_r^1(\omega)e^{j\omega t_r^1} - A_r^2(\omega)e^{j\omega t_r^2}, \tag{2}$$

where A_r^1 and t_r^1 are the amplitude and travel time of the D arrival, respectively. Similarly, A_r^2 and t_r^2 are for the SR arrival. Generally, one can assume[13]

$$A_r^1(\omega) \approx A_r^2(\omega), \tag{3}$$

then the sound intensity can be obtained as

$$|p_r(\omega)|^2 = 2A_r^1(\omega)^2[1 - \cos(\omega\Delta t_r)], \tag{4}$$

where $\Delta t_r = t_r^2 - t_r^1$ is the relative time delay (RTD) of D and SR arrivals.

Due to the fact that the travel time of D and SR arrivals is barely affected by the angular frequency, when deducing the analytical expression of horizontal–longitudinal correlation coefficient based on the ray method, the frequency factor can focus on the central angular frequency ω_0. The frequency dependence of horizontal–longitudinal correlation coefficient will be discussed in the following. Thus Eq. (1) can be expressed as

$$\begin{aligned}\rho(r, r+\Delta r) &\approx \max_\tau \frac{\Delta\omega \mathrm{Re}(p_r(\omega_0)p_{r+\Delta r}^*(\omega_0)e^{i\omega_0\tau})}{\sqrt{(\Delta\omega)^2|p_r(\omega_0)|^2|p_{r+\Delta r}(\omega_0)|^2}} \\ &= \max_\tau \frac{\mathrm{Re}(p_r(\omega_0)p_{r+\Delta r}^*(\omega_0)e^{i\omega_0\tau})}{|p_r(\omega_0)||p_{r+\Delta r}(\omega_0)|},\end{aligned} \tag{5}$$

where $\Delta\omega = \omega_1 - \omega_2$. Ignoring the amplitude variation of D and SR arrivals, the cross correlation of the complex pressure field can be expressed as

$$\begin{aligned}&p_r(\omega_0)p_{r+\Delta r}^*(\omega_0)e^{i\omega_0\tau} \\ &\approx A_r^1 A_{r+\Delta r}^1 e^{j\omega_0(t_r^1 - t_{r+\Delta r}^1 + \tau)}(1 \\ &\quad - e^{j\omega_0\Delta t_r})(1 - e^{-j\omega_0\Delta t_{r+\Delta r}}).\end{aligned} \tag{6}$$

In practice, when the horizontal–longitudinal correlation coefficient of the acoustic field reaches maxima by adjusting τ, one obtains

$$t_r^1 - t_{r+\Delta r}^1 + \tau \approx 0. \tag{7}$$

Then, the numerator in Eq. (5) becomes

$$\begin{aligned}&\max_\tau \mathrm{Re}(p_r(\omega_0)p_{r+\Delta r}^*(\omega_0)e^{i\omega_0\tau}) \\ &= A_r^1 A_{r+\Delta r}^1[1 + \cos(\omega_0(\Delta t_r - \Delta t_{r+\Delta r})) \\ &\quad - \cos(\omega_0\Delta t_r) - \cos(\omega_0\Delta t_{r+\Delta r})].\end{aligned} \tag{8}$$

Using similar derivation, the denominator in Eq. (5) is given by

$$\begin{aligned}&|p_r(\omega_0)||p_{r+\Delta r}(\omega_0)| \\ &= 2A_r^1 A_{r+\Delta r}^1 \sqrt{(1 - \cos(\omega_0\Delta t_r))(1 - \cos(\omega_0\Delta t_{r+\Delta r}))}.\end{aligned} \tag{9}$$

According to the addition theorem of trigonometric function, Eq. (5) becomes

$$\begin{aligned}&\rho(r, r+\Delta r) \\ &= \frac{1}{2}\sqrt{(1 - \cos(\omega_0\Delta t_r))(1 - \cos(\omega_0\Delta t_{r+\Delta r}))} \\ &\quad + \frac{1}{2}\frac{\sin(\omega_0\Delta t_r)\sin(\omega_0\Delta t_{r+\Delta r})}{\sqrt{(1 - \cos(\omega_0\Delta t_r))(1 - \cos(\omega_0\Delta t_{r+\Delta r}))}}.\end{aligned} \tag{10}$$

Last, using the half-angle and double-angle formulae, Eq. (10) becomes

$$\begin{aligned}\rho(r, r+\Delta r) &= \sin\frac{\omega_0\Delta t_r}{2}\sin\frac{\omega_0\Delta t_{r+\Delta r}}{2} \\ &\quad + \cos\frac{\omega_0\Delta t_r}{2}\cos\frac{\omega_0\Delta t_{r+\Delta r}}{2} \\ &= \cos\frac{\omega_0(\Delta t_r - \Delta t_{r+\Delta r})}{2}.\end{aligned} \tag{11}$$

So far, the analytical solution of the horizontal–longitudinal correlation coefficient has been obtained. It strongly relies on the central frequency ω_0 and the distribution of RTDs. Now we first study the dependence of horizontal–longitudinal correlation coefficient on the source depth.

Simulation data by using BELLHOP were generated to calculate the horizontal–longitudinal correlation coefficient for different source-receiver geometries. In the simulation, the central frequency is 310 Hz with the bandwidth of 100 Hz.

The simulated horizontal–longitudinal correlation coefficients for different source depths are shown in Fig. 2. The source depths for Figs. 2(a)–2(d) are 50, 100, 150 and 200 m, respectively. The horizontal axis

represents the receiver range, and the vertical axis depicts the horizontal–longitudinal separation, Δr. If the horizontal–longitudinal correlation length is defined as the longitudinal separation at which the correlation coefficient decays to 0.707,[7] the superimposed dashed lines in Fig. 2 indicate the correlation lengths for different conditions.

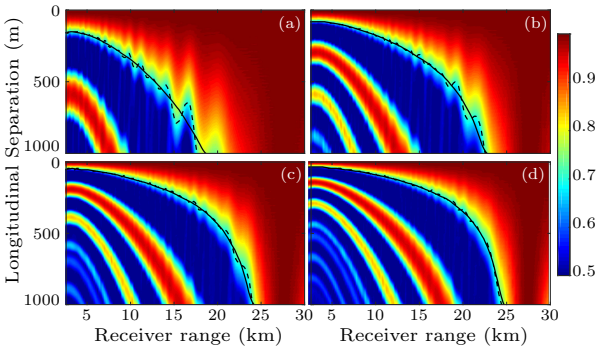

Fig. 2. Horizontal–longitudinal correlation coefficient as functions of the receiver range and horizontal–longitudinal separation with source depths of (a) 50 m, (b) 100 m, (c) 150 m and (d) 200 m. The receiver depth is 4700 m.

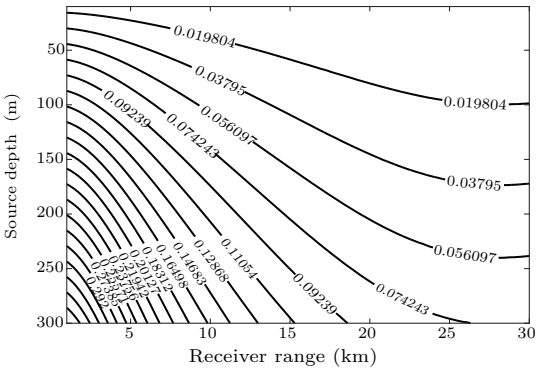

Fig. 3. The distribution of RTDs as functions of the receiver range and the source depth. The receiver depth is 4700 m. The unit of time delay is the second.

To verify the validity of Eq. (11), the distribution of RTDs at the receiver depth of 4700 m by applying the software BELLHOP is shown in Fig. 3. At the same source depth, the gradient of RTD variation decreases as the receiver range increases. The shallower source shows smaller RTD span than the deeper one over the same receiver range interval. Using Eq. (11), the analytical solutions of horizontal–longitudinal correlation coefficients are superimposed on Fig. 2 with black solid lines, where f_0 ($\omega_0 = 2\pi f_0$) is 310 Hz. One can see that the analytical solutions of horizontal–longitudinal correlation lengths are generally coincident with the numerical results. Moreover, three important features of variation of spatial correlation shown in Fig. 2 are as follows: (1) In the certain receiver range, the horizontal–longitudinal correlation length increases as the source depth decreases. (2) For the same source depth, the horizontal–longitudinal correlation length increases with the increasing receiver range. (3) The horizontal–longitudinal correlation coefficient is oscillating along longitudinal separation. In the large receiver range, especially for the shallow source, the correlation length also oscillates with the receiver range.

In terms of the real application, the effect of the receiver depth on the horizontal–longitudinal correlation coefficient is also investigated as shown in Fig. 4. The source depth is 100 m. The receiver depths for Figs 4(a)–4(d) are 4600, 4800, 4900 and 5000 m, respectively. One can find that the receiver depths have slight influence on the variability of correlation coefficients. Due to the bottom-interacting effect and possible model error, the variation of horizontal–longitudinal spatial correlation has slight perturbation for the 5000 m receiver depth, but the basic law is not changed. Referring back to Fig. 1, one also notices that the interference structure of acoustic field at depth above 4600 m changes with the depth slowly.

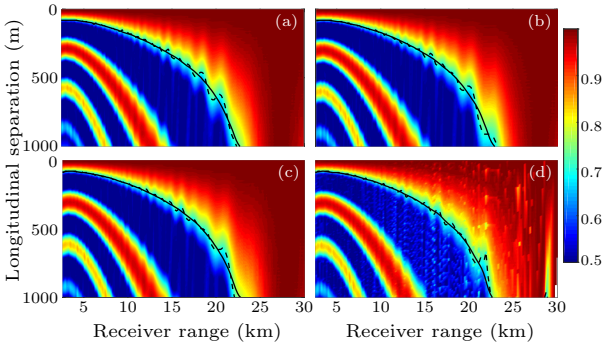

Fig. 4. Horizontal–longitudinal correlation coefficient as functions of receiver range and horizontal–longitudinal separation with receiver depths of (a) 4600 m, (b) 4800 m, (c) 4900 m and (d) 5000 m. The source depth is 100 m.

To see the variability of horizontal–longitudinal spatial correlation, one should refer back to the image theory. The total field can be written as[14]

$$p(r,z) = -\frac{2i}{R}\sin(kz_{\rm s}\sin\theta)e^{ikR}, \tag{12}$$

where $R = \sqrt{r^2+z^2}$ is the slant range from the image origin to the receiver, $\theta = \tan^{-1}(z/r)$ is the declination angle, $k = \omega/c$ is the wave number, and $z_{\rm s}$ is the source depth. The amplitude variation takes the simple form

$$|p| = \frac{2}{R}|\sin(kz_{\rm s}\sin\theta)|, \tag{13}$$

which accounts for the interference pattern as shown in Fig. 1.

The horizontal–longitudinal spatial correlation of acoustic field at two different ranges is closely associated with the interference results of D and SR arrivals in these two ranges. If both of them are constructive or destructive interference, the horizontal–longitudinal correlation coefficient would be high. Contour plots of TL, mapped in range and frequency, exhibit slanted striations as shown in Fig. 5.

In a certain receiver range, the acoustic intensity is oscillating with the frequency. Due to the fact that

the striations are slanted, the peaks and valleys of acoustic intensity occur at different frequency bins for two different receiver ranges. When the peaks and valleys of acoustic intensity in the two different ranges reach an agreement, the horizontal–longitudinal correlation coefficient will be high. In short ranges, the variation speed of oscillation is fast and leads to quick variation of horizontal–longitudinal spatial correlation and small horizontal–longitudinal correlation length whereas it slows down and leads to large correlation lengths in large ranges.

As the source depth becomes deeper, the period of interference oscillation along horizontal–longitudinal range becomes shorter as indicated by Eq. (13), as shown in Fig. 5(b). According to the above explanation, the variation of horizontal–longitudinal spatial correlation goes fast and the horizontal–longitudinal correlation length decreases.

Furthermore, in long ranges the number of striations is few for the shallow source. The small number of interference striations will lead to a weak frequency-dependent smoothing effect, and consequently the horizontal–longitudinal correlation lengths will be oscillatory along the receiver range as shown in Fig. 2(a).

Moreover, if the striations are vertical, the horizontal–longitudinal correlation lengths would oscillate with the periods comparable with the width of interference striations. If the striations are horizontal, the horizontal–longitudinal correlation coefficient would keep constant. In Figs 2 and 4, we can see that the horizontal–longitudinal correlation coefficients are high in the vicinity of 1/2 convergence zone, which in fact are consistent with Ref. [7].

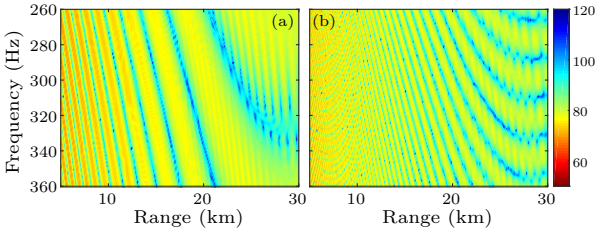

Fig. 5. TL as functions of range and frequency at receiver of 4700 m with source depths of (a) 50 m and (b) 200 m.

Except for the source depth, the central angular frequency and the bandwidth are the key factors impacting on the variability of horizontal–longitudinal spatial correlation of acoustic field. Figure 6 gives both numerical simulation results and the theoretical analytical solutions of horizontal–longitudinal correlation lengths for different scenes. The central frequencies for Figs 6(a) and 6(b) are 310 Hz with bandwidth of 60 Hz and the source depths are 100 and 300 m, respectively. Figures 6(c) and 6(d) are the high frequency results. The central frequencies are 1150 Hz with bandwidth of 300 Hz and the source depths are 30 and 100 m, respectively. For the low frequency scene, comparing Fig. 2(b) with Fig. 6(a), one can find that when the bandwidth decreases, the oscillation becomes serious. This is because the number of striations becomes small when the bandwidth decreases. However, when the source depth increases to 300 m as shown in Fig. 6(b), the situation has been improved due to the increasing number of striations. For the high frequency scene as shown in Figs 6(c) and 6(d), the variability of horizontal–longitudinal spatial correlation is equal to that under the low frequency scene.

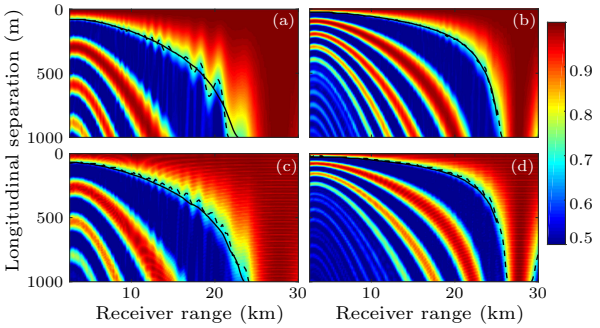

Fig. 6. Horizontal–longitudinal correlation coefficient for different scenes at receiver depth of 4700 m with (a) source depth of 100 m and frequency band of 280–340 Hz, (b) source depth of 300 m and frequency band of 280–340 Hz, (c) source depth of 30 m and frequency band of 1000–1300 Hz, and (d) source depth of 100 m and frequency band of 1000–1300 Hz.

As a note, the analytical expression of the horizontal–longitudinal spatial correlation is suitable for both low and high frequencies. The horizontal–longitudinal spatial correlation is associated with the source depth, central frequency and bandwidth of the acoustic field, all of which decide the number of interference striations and the evolution speed of the interference oscillation. As long as the number of slanted interference striations over the bandwidth of interest is large enough, Eq. (11) can predict the variation of horizontal–longitudinal correlation lengths well.

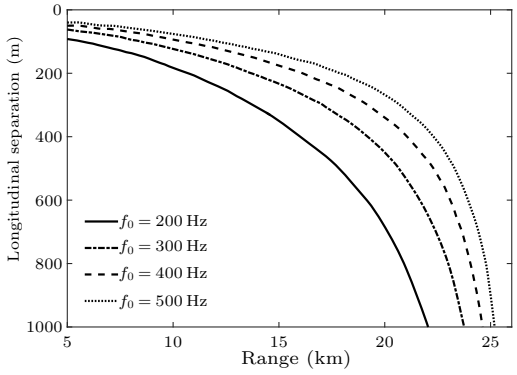

Fig. 7. Theoretical correlation lengths for different frequencies with the source depth of 150 m and the receiver depth of 4700 m.

Lastly, one should bear in mind that the choice of ω_0 in Eq. (11) is conditioned. The variation of horizontal–longitudinal correlation lengths for different center frequencies in Eq. (11) is shown in Fig. 7 with the source depth of 150 m and the receiver depth of 4700 m. The lower the frequency is, the larger the variation scope of horizontal–longitudinal correlation length over the same bandwidth is. In fact,

the horizontal–longitudinal correlation length, obtained by Eq. (11) using the lower frequency boundary ω_1 in Eq. (1), corresponds to the maximum value of the correlation length. Usually, the central angular frequency ω_0 is suggested to be used as the reference value for the calculation of the theoretical value of the horizontal–longitudinal correlation length.

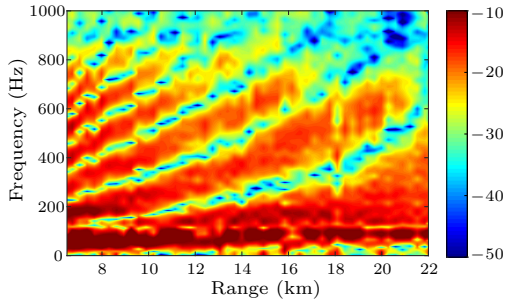

Fig. 8. Contour plots of the received acoustic intensity mapped in range and frequency. The color scale is in decibels.

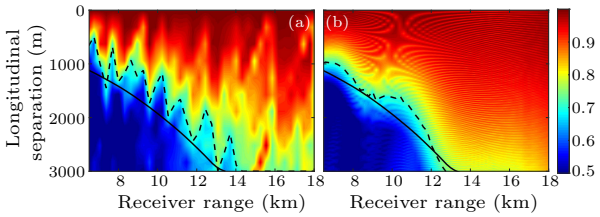

Fig. 9. Comparison of horizontal–longitudinal correlation coefficients estimated from (a) experimental data and (b) numerical modeling.

The experiment was performed in the West Pacific Ocean, where the ocean bottom is almost flat with depth of about 4500 m. A bottom-moored hydrophone was deployed at 4200 m depth. When the ship was moving away from the hydrophone, an air gun source was towed at a depth of about 10 m. The towed speed was about 1.935 m/s. The air gun signal was generated with the time interval of 160 s. The first signal was generated in the range of 6.16 km. The contour plots of the acoustic intensity, mapped in range and frequency, are shown in Fig. 8. When the source range was farther than 21 km, there were no clear striations along frequency due to the small time delay of D and SR arrivals. The frequency band used for estimating the correlation coefficients was from 200 to 600 Hz. The processing results of horizontal–longitudinal correlation coefficients are shown in Fig. 9(a). The dashed line indicates the horizontal–longitudinal correlation lengths in different receiver ranges. The solid line is predicated by Eq. (11) with $f_0 = 400$ Hz. For comparison, Fig. 9(b) shows the results by numerical modeling. We can find that the experimental results are in good agreement with the numerical results. The analytical solution can also describe the variation of horizontal–longitudinal correlation length well.

In summary, the horizontal–longitudinal correlation of acoustic field has been analyzed by numerical modeling and theoretical derivation under RAP environment. The horizontal–longitudinal spatial correlation is closely related to the source depth, central frequency, as well as the bandwidth of broadband acoustic field. The variability of horizontal–longitudinal spatial correlation is dependent on the interference structure of acoustic field, including the number and slope of striations and the evolution speed of interference structure along ranges. The analytical solution can be used for guiding the design of bottom-moored array and the estimation of integral time for moving source localization.

References

[1] Gorodetskaya E U et al 1999 *IEEE J. Oceanic Eng.* **24** 156
[2] Yang T C 2006 *J. Acoust. Soc. Am.* **120** 2595
[3] Yang T C 2008 *J. Acoust. Soc. Am.* **124** 113
[4] Spiesberger J L 2009 *J. Acoust. Soc. Am.* **126** 70
[5] Colosi J A et al 2013 *J. Acoust. Soc. Am.* **134** 3119
[6] Wu L L and Peng Z H 2015 *Chin. Phys. Lett.* **32** 094302
[7] Li J, Li Z L, Ren Y et al 2015 *Chin. Phys. Lett.* **32** 064303
[8] Duan R, Yang K D, Ma Y L et al 2012 *Chin. Phys.* B **21** 124301
[9] McCargar R and Zurk L M 2013 *J. Acoust. Soc. Am.* **133** EL320
[10] Duan R, Yang K D, Ma Y L et al 2014 *J. Acoust. Soc. Am.* **136** EL159
[11] Lei Z X, Yang K D and Ma Y L 2016 *J. Acoust. Soc. Am.* **139** EL196
[12] Porter M B 2011 *BELLHOP Manual User's Guide* p 45
[13] Weng J B, Li F H and Guo Y G 2016 *Acta Acust.* **41** 3
[14] Jensen F B, Kuperman W A et al 2011 *Computational Ocean Acoustics* 2nd edn (New York: Springer)